Hindawi
Mathematical Problems in Engineering
Volume 2021, Article ID 6673612, 17 pages
https://doi.org/10.1155/2021/6673612

Research Article

Optimization Analysis of Engine Intake System Based on Coupling Matlab-Simulink with GT-Power

Feng Jiang,[1,2,3] **Minghai Li**,[1] **Jiayan Wen**,[2,3] **Zedan Tan**,[2] **and Wenyun Zhou**[2]

[1]*Internal Combustion Engine Research Institute, Dalian JiaoTong University, Dalian 116028, China*
[2]*College of Electrical and Information Engineering, Guangxi University of Science and Technology, Liuzhou 545006, China*
[3]*Guangxi Key Laboratory of Automobile Components and Vehicle Technology, Liuzhou 545006, China*

Correspondence should be addressed to Jiayan Wen; wenjiayan2012@126.com

Received 13 November 2020; Revised 8 March 2021; Accepted 22 March 2021; Published 9 April 2021

Academic Editor: Seralathan Sivamani

In the work, the suitable volumetric efficiency is very important for the gasoline engine to achieve the aim of energy-saving and emission reduction. Thus, the intake system characteristics, such as intake manifold length, diameter, volumetric efficiency, and valve phase, should be investigated in detail. In order to investigate the performance optimization of the engine intake system, an optimization model of the engine intake system is developed by the GT-Power coupled with Matlab-Simulink and validated by the experimental results under the different conditions at full load. The engine power-, torque-, and brake-specific fuel consumption are defined as the result variables of the optimization model, and the length and diameter of the intake manifold are defined as the independent variables of the model. The results show that the length of intake manifold has little influence on the engine power and BSFC, and the length of intake manifold has a great impact on the performance index at high speed. In addition, the engine volumetric efficiency is the highest when the length of intake manifold is in the range of 240 and 250 mm. The engine BSFC improved by variable valve timing is significant compared with the original result. Finally, the improvement suggestions for the performance enhancement of the gasoline engine are proposed.

1. Introduction

With the great challenges of global energy crisis and environmental pollution [1], realizing the energy conservation and emission reduction and improving the performance of the engine have already formed the broad consensus [2]. Thus, in many countries, more strict regulations and relevant countermeasures are issued for the problem in recent years [3]. To further optimize the performance of gasoline engine, it is necessary to investigate the knowledge of in-cylinder phenomena including chemical kinetics that determine emissions formation [4], temporally and spatially varying in-cylinder charge conditions, heat release rates [5], EGR [6], and selective catalyst reduction [7]. Similarly, lots of experts and scholars do a lot of studies, and many new technologies have been proposed for improving the engine combustion [8–10]. Improving the gasoline engine combustion is the main way to improve the engine power and reduce emissions [11]. The intake and exhaust system, fuel supply system, and combustion chamber shape are the key factors to determine the combustion process [12].

In order to improve the combustion and reduce the pollution emissions, the sufficient fresh air should be allowed to enter the cylinder and enhance the quality of the mixture [13]. This required that the intake system should be investigated and optimized [14]. In general, the structure parameter and valve timing of the intake have a great influence on the gas flow performance [15]. It is very necessary to carry out the research on the performance of intake and exhaust system in both theory and practice. More specifically, a well-designed intake and exhaust system is beneficial for the improvement of volumetric efficiency and the reduction in the BSFC and emissions when the engine is in a certain speed range [16,17]. The fresh air enters the engine cylinder through the intake system in the form of pressure wave transmission and mixes quickly with fuel [18,19]. The

volumetric efficiency is the principal factor that has an effect on the engine power and is considered as an important evaluation index of the intake system [20]. Therefore, it is very important to optimize the intake system to meet the requirements of energy saving and emission reduction [21]. The variable air intake system can make the engine air intake system suitable for the wide speed range. In addition, the suitable volumetric efficiency can improve the good performance at different conditions, and it will be helpful for the improvement of engine power, torque, and fuel consumption and emissions [22–24]. Therefore, it is of great significance to optimize the intake system and valve timing of the engine [25].

In recent years, many researchers have engaged in the optimization analysis of the engine intake system. For instance, Yang et al. had developed a GT-Power model of engine intake system and analyzed the effect of harmonic on intake system. In addition, the response surface method is employed to optimize the intake system [26]. Qi et al. had developed a CFD model with the KIVA and STAR-CD software and analyzed the temperature, concentration, and flow field in engine cylinder; then, the intake system was optimized based on the relationship between the structure of intake system and in-cylinder flow [27]. Similarly, Pai et al. [28] established an engine simulation model with the GT-Power and STAR-CD software and investigated the effect of the engine intake system on the engine performance. The result indicated that the engine performance had been improved clearly. In addition, Silva et al. [29] had established an engine simulation model with the GT-Power model. The model was employed to analyze the relationship between the volumetric efficiency and the geometric parameters of the intake manifold by the Brent method and optimized the intake system. Guo et al. [30] had proposed an optimization design method for the engine intake manifold based on reverse engineering and CFD software. They found that the proposed technology was reasonable for the intake manifold optimized design. Carvalho et al. [31] had established a thermodynamic model of the engine in GT-Suite environment and focused on the optimization tool for DoE (Design of Experiment). They found that the volumetric efficiency of the engine had been greatly improved. Sun et al. [32] proposed an optimization analysis method to optimize the design of the engine inlet based on the coupling of genetic algorithm and artificial neural network. The results indicated that the flow performance of the engine inlet was improved. Wang [33] used the design of six sigma (DFSS) methodology to optimize the engine intake and exhaust system. The results showed that the optimized emission performance complied with emission regulations, and the fuel economy was significantly improved.

As it is mentioned, the numerical simulation of internal-combustion engine has obvious advantages and is regarded as a very effective tool for saving experimental costs through the detailed mathematical framework [34–36]. In the paper, an innovative optimization model is employed to simulate the intake combustion processes. Firstly, the model was developed and then validated by the experimental results under the different conditions at full load. Finally, the optimization model method was firstly used to optimize the performance of ethanol-gasoline engine. The findings are of interest due to both prevention of performance losses and emission reduction using the suitable volumetric efficiency.

2. Mathematical Model

The mathematical model of four-cylinder gasoline engine was developed by GT-Power coupled with Matlab-Simulink and was employed to study the optimization. The models involve the combustion model, intake pressure wave model, and intake system optimization model [15]. In addition, the air and exhaust gas are considered as the ideal gas. Thus, the gas properties depend on temperature and gas composition.

2.1. Combustion Model. The zero-dimensional combustion model is employed to investigate the combustion in cylinder. The energy conservation equation of the combustion process is summarized as follows [5]:

$$\frac{dQ_B}{dv\varphi} = \frac{dU}{d\varphi} + \frac{dW}{d\varphi} + \frac{dQ_w}{d\varphi}, \tag{1}$$

where U is the internal energy of the system, which is determined by the mass and temperature change in the medium in the combustion chamber; W is the mechanical work acting on the piston, which is usually closely related to the output power and torque of the cylinder; Q_w is the heat transfer through the system boundary; Q_B is the heat released by the combustion of working fluid in the cylinder, which is usually determined by the fuel mass; and φ is the instantaneous timing angle.

The heat transfer Q_w can be predicted by the following equation:

$$\frac{dQ_w}{d\varphi} = \sum_{i=1}^{3} \frac{dQ_{wi}}{d\varphi} = \frac{\alpha_g}{\omega} \sum_{i=1}^{3} A_i (T - T_{wi}), \tag{2}$$

where of working fluid to the walls of combustion chamber such as the bottom surface of the cylinder head ($i = 1$), the top surface of the piston ($i = 2$), and the surface of the cylinder liner ($i = 3$), which are determined by the average wall temperature T_w, the instantaneous average heat transfer coefficient α_g of the working fluid to the surrounding wall of combustion chamber, the crankshaft speed ω, the heat exchange area A, and the instantaneous temperature T of the working fluid inside the cylinder.

The average heat transfer coefficient α_g can be obtained by the following equation:

$$\alpha_g = 820 p^{0.8} \cdot T^{-0.53} \cdot D^{-0.2} \cdot \left[C_1 \cdot C_m + C_2 \frac{T_a V_s}{p_a V_a} (p - p_0) \right]^{0.8}, \tag{3}$$

where p is the working fluid pressure in the cylinder; D is the cylinder diameter; C_m is the average piston speed; p_a, T_a, and V_a are the working fluid pressure, temperature, and cylinder volume in the cylinder at the starting point of compression, respectively; V_s is the cylinder working volume; p_o is the cylinder pressure when the engine is motoring; C_1 is the

velocity coefficient; and C_2 is the combustion chamber status quo coefficient.

During the combustion process, the medium inside the cylinder meets the following mass conservation equation:

$$\frac{dm}{d\varphi} = \frac{dm_s}{d\varphi} + \frac{dm_e}{d\varphi} + g_f \cdot \frac{dX}{d\varphi}, \tag{4}$$

where m is the mass of working fluid in the system; m_s is the mass of air flowing into the cylinder; m_e is the mass of exhaust gas flowing out of the cylinder; g_f is the circulating fuel injection quantity of the engine; X is the percentage of fuel combustion in the cylinder, and $X = (m_B/g_f) \times 100\%$; and m_B is the instantaneous fuel mass injected into the cylinder.

Based on the Weber function model, the semiempirical equation can be obtained by the following equation:

$$\frac{dX}{d\varphi} = 6.908 \frac{M+1}{\varphi_z} \cdot \left[\frac{\varphi - \varphi_b}{\varphi_z}\right] \cdot e^{-6.908 \cdot \left[(\varphi - \varphi_b)/\varphi_z\right]^{M+1}}, \tag{5}$$

where M is the combustion quality index, $\varphi_z = \varphi_b - \varphi_c$ is the combustion duration angle, φ_b is the combustion start angle, and φ_c is the combustion end angle.

Furthermore, during the combustion process, the working fluid inside the cylinder shows the following ideal gas state equation:

$$pV = mRT, \tag{6}$$

where V is the volume of working fluid in the system, respectively, and R is the gas constant.

The output power P_e is organized as follows:

$$P_e = k\eta\omega \frac{dW}{d\varphi} = \frac{k\eta T_{tq} n}{9550}, \tag{7}$$

where n is the engine speed, η is the mechanical efficiency, and k is the cylinder number.

However, during the intake and exhaust strokes, the gas flow process in intake and exhaust manifolds is very complex and has the typical unsteady flow characteristics. This unsteady flow often leads to very strong pressure fluctuations at the manifold and cylinder valves. Furthermore, it will affect the thermal process and has a greater impact on the air exchange quality, combustion efficiency, output power, and torque in the cylinder. To obtain the comprehensive thermal parameters of the whole machine, it usually ignored the pressure transmission in the intake pipe. Thus, the mass of the working fluid discharged from the cylinder into the intake pipe can be obtained by the following equation:

$$\frac{dm_{3A}}{d\varphi} = \frac{\mu_3 F_3}{\omega} \sqrt{p_3 \rho_3} \cdot \sqrt{\frac{2\kappa_3}{\kappa_3 - 1}\left[\left(\frac{p_0}{p_3}\right)^{2/\kappa_3} - \left(\frac{p_0}{p_3}\right)^{(\kappa_3+1)/\kappa_3}\right]}, \tag{8}$$

where m_{3A} is the mass of the working fluid discharged from the cylinder into the intake pipe; μ_3 is the gas flow coefficient of the intake pipe, which is measured by experiment; F_3 is the cross-sectional area of the intake pipe outlet; ρ_3 is the gas density in the intake pipe; κ_3 is the specific heat capacity ratio of the gas in the intake pipe; and p_3 is the gas pressure in the intake pipe.

2.2. Intake Pressure Wave Model. Natural frequency of pressure wave f_1 can be obtained by the following equation:

$$f_1 = \frac{a}{4L}, \tag{9}$$

where a is the sound velocity of the gas in intake pipe and L is the intake pipe equivalent length.

When engine speed is n (r/min), the volumetric frequency f_2 can be calculated by the following equation:

$$f_2 = \frac{n}{60 \times 2}. \tag{10}$$

The ratio of f_1 to f_2 is q_1, which shows the relationship between the natural frequency of pressure wave in intake manifold and engine intake frequency. Thus, the wave effect can be obtained by the following equation:

$$q_1 = \frac{f_1}{f_2} = \frac{30a}{nL}. \tag{11}$$

When $q_1 = 1\,(1/2), 2\,(1/2)\ldots\ldots$, the inlet air coincides with the positive pressure wave during the next valve opening. Thus, the volumetric efficiency increases. When $q_1 = 1,\ 2,\ \ldots\ldots$, the intake frequency coincides with the natural frequency of the pressure wave, and during the next valve opening, inlet air coincides with the negative pressure wave. Thus, the volumetric efficiency decreases.

The smaller the q_1, the longer the intake pipe; the larger the q_1, the larger the pressure wave attenuation due to the friction. Equation (11) shows that if q_1 is fixed, the length of the pipe is inversely proportional to the engine speed.

It can be seen that the reasonable length of intake pipe, diameter, and volume is beneficial to improving the mixture of fuel and fresh air, resulting in the increase in engine power. Pressure wave shows variations in the pipeline. It can be calculated according to the one-dimensional unsteady flow of gas in the pipeline. Generally speaking, the structural size of the pipeline can be determined by the combination of simulation and experiment.

2.3. Optimization Model of Intake System. In the paper, the Brent method is employed to carry out the optimization of intake system. When other parameters are fixed, P_e can be written as a function of the intake pipe radius R_a and length L:

$$\begin{aligned} P_e &= f_1(x), \\ x &= [R_a, L]^T. \end{aligned} \tag{12}$$

When the length and diameter of the intake pipe change, the output power also changes. According to the optimization theory and the algorithms, the following optimization model can be established:

$$\begin{aligned} &\min P_e = f_1(x), \\ &\text{st.} \quad 26 \le x(1) \le 42, \\ &\qquad 200 \le x(2) \le 280. \end{aligned} \tag{13}$$

After determining the optimal intake pipe parameter, the intake and exhaust valve timing angles φ_B and φ_C can be further optimized. The optimization mathematical model can be written as

$$\begin{aligned} &\min P_e = f_2(\overline{x}), \quad \overline{x} = [\varphi_B, \varphi_C]^T, \\ &\text{st.} \quad 115 \le \overline{x}(1) \le 135, \\ &\qquad 224.5 \le \overline{x}(2) \le 244.5. \end{aligned} \tag{14}$$

According to the optimization theory, the x_0 is defined as the initial search point. It is not difficult to determine that its negative gradient direction is the direction in which the function value drops the fastest. As previously mentioned, the new search point is determined as

$$x_1 = x_0 - \alpha_0 \nabla f_1(x_0). \tag{15}$$

When the value of the positive real number α_o is different, the new search point obtained is different. Similarly, the function value of $f_1(x_1)$ will also be different. As shown in Figure 1, the different values of $x_1^{(0)}$ and $x_1^{(1)}$ are obtained at different α_0^0 and α_0^1. The value of $f_1(x_1)$ will change with the variable α_o and is defined as $f_1(x_1) = \psi_1(\alpha_0)$. In order to obtain the minimum value of $f_1(x)$, the extreme value of all the function values should be obtained by the following equation:

$$\frac{\partial \psi_1(\alpha_0)}{\partial \alpha_0} = g(\alpha_0) = 0. \tag{16}$$

The Brent method is a faster search method which combines dichotomy, linear interpolation, and inverse quadratic interpolation together. In the paper, the Brent method is employed to seek the solution of equation (16) in the GT-Power environment. The specific steps are as follows.

Firstly, the initialization interval of the variable α_o is defined as $[a, b]$. If it is $g(a_0) \cdot g(b_0) < 0$, the estimated value of iterative root of the step k is marked as $\alpha_0^k = b_k$. If it is $|g(a_k)| < |g(b_k)|$, the estimated value of iterative root of the step k is marked as $\alpha_0^k = a_k$. Then, the estimated values of iterative roots of the first two steps are marked as b_{k-1} and b_{k-2}, respectively, and judge whether the following four inequalities are true:

$$|\delta| < |b_k - b_{k-1}|, \tag{17a}$$

$$|\delta| < |b_{k-1} - b_{k-2}|, \tag{17b}$$

$$|s - b_k| < \frac{1}{2}|b_k - b_{k-1}|, \quad s = a_k \text{ or } b_k, \tag{17c}$$

$$|s - b_k| < \frac{1}{2}|b_{k-1} - b_{k-2}|. \tag{17d}$$

Let us see whether the following five conditions are true or false:

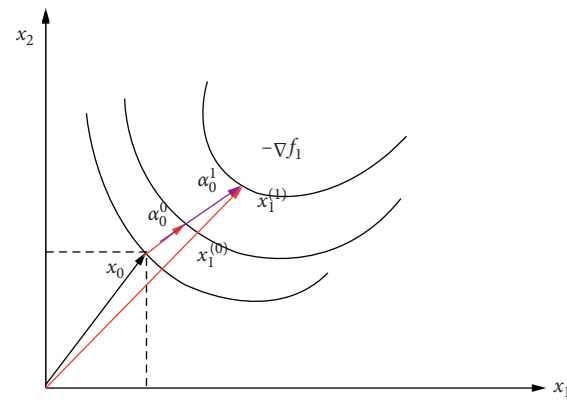

Figure 1: Schematic diagram of one-dimensional search method.

(1) The step $k-1$ iteration is dichotomy and (17a) is not true.

(2) The step $k-1$ iteration is dichotomy and (17c) is not true.

(3) The step $k-1$ iteration is interpolation method and (17b) is not true.

(4) The step $k-1$ iteration is interpolation method and (17d) is not true.

(5) The temporary value calculated by the interpolation method is not in the interval $[((3a_k + b_k)/4), b_k]$.

If one of the above five conditions is true, the iterative value α_o^{k+1} of the current root can be obtained by dichotomy:

$$\alpha_0^{k+1} = \frac{1}{2}(a_k + b_k). \tag{18}$$

If none of the above conditions is true, let us try the following equation:

$$\begin{aligned} &\alpha_0^{k-1} \ne \alpha_0^k, \\ &\alpha_0^{k-1} \ne \alpha_0^{k+1}, \\ &\alpha_0^k \ne \alpha_0^{k+1}. \end{aligned} \tag{19}$$

If equation (19) is true, then do the following step:

$$\begin{aligned} \alpha_0^{k+1} = {} & \frac{g(\alpha_0^{k-1})g(\alpha_0^k)}{(g(\alpha_0^{k-2}) - g(\alpha_0^{k-1}))(g(\alpha_0^{k-2}) - g(\alpha_0^k))}\alpha_0^{k-2} \\ & + \frac{g(\alpha_0^{k-2})g(\alpha_0^{k-1})}{(g(\alpha_0^k) - g(\alpha_0^{k-2}))(g(\alpha_0^k) - g(\alpha_0^{k-2}))}\alpha_0^k \\ & + \frac{g(\alpha_0^{k-2})g(\alpha_0^k)}{(g(\alpha_0^{k-1}) - g(\alpha_0^{k-2}))(g(\alpha_0^{k-1}) - g(\alpha_0^k))}\alpha_0^{k-1}. \end{aligned} \tag{20}$$

If equation (19) is not true, then do the following step:

$$\alpha_0^{k+1} = b_k - \frac{(b_k - a_k)g(b_k)}{g(b_k) - g(a_k)}. \tag{21}$$

It should be pointed out that the temporary value $s = \alpha_o^{k+1}$ in equations (17c) and (17d); after each iteration is completed, the root interval $[a_k, b_k]$ will be further reduced to $[a_{k+1}, b_{k+1}]$, where $a_{k+1} = s$ or $b_{k+1} = s$; the other end point is one of a_k and b_k and meets

$$g(a_{k+1}) \cdot g(b_{k+1}) < 0, \quad |g(a_{k+1})| > |g(b_{k+1})|. \tag{22}$$

Repeat the above iterations until α_o converges to zero; that is to say, the interval length of the solution tends to an infinitesimal value. It can be expressed as

$$|a_{k+1} - b_{k+1}| \le \varepsilon_1. \tag{23}$$

By analogy, it is not difficult to construct a sequence of iteration points as follows:

$$x_{k+1} = x_k - \alpha_k \nabla f_1(x_k), \quad (k = 1, 2, \ldots). \tag{24}$$

In addition, the positive real number α_k can be determined according to the following equation:

$$\frac{\partial \psi_1(\alpha_k)}{\partial \alpha_k} = 0, \tag{25}$$

until the sequence meets the following convergence conditions:

$$\|x_{k+1} - x_k\| \le \varepsilon, \tag{26}$$

where $\|\cdot\|$ is the norm of the vector and ε is a minimal positive real value.

2.4. Optimization Model. In the paper, the optimization model of the engine intake system is developed by the GT-Power coupled with Matlab-Simulink. The acceptable curves of optimization model are shown in Figure 2. When the result variable reaches the maximum or minimum, its variation must meet the following trend: the result firstly increases and reaches a maximum and then decreases with the increase in the independent variable, or the result firstly decreases and reaches a minimum and then increases with the increase in the independent variable.

The core of the optimization model is composed of nonlinear constrained optimization and discrete grid method. The optimization of engine in engineering field is realized by this mathematical method. Discrete grid method is an optimization algorithm based on the idea of Brent method [24].

According to the given objective function and constraints, the optimization model is established, and the corresponding optimization design is carried out. In the optimization model, the objective function is defined as the design variables of a real-time variable (RLT variables). A series of optimal design vector sequences are generated when the appropriate iteration method is used. When the sequence converges, it reaches the optimal solution.

By analyzing the influences of intake manifold length, diameter, and other factors on the performance of gasoline (E10) engine fueled with ethanol, it is found that the parameters of intake manifold length, diameter, and valve timing are beneficial to the optimization of engine performance. On this basis, the volumetric efficiency is defined as the optimization objective. The intake manifold length, diameter, and valve timing are defined as the optimization independent variables.

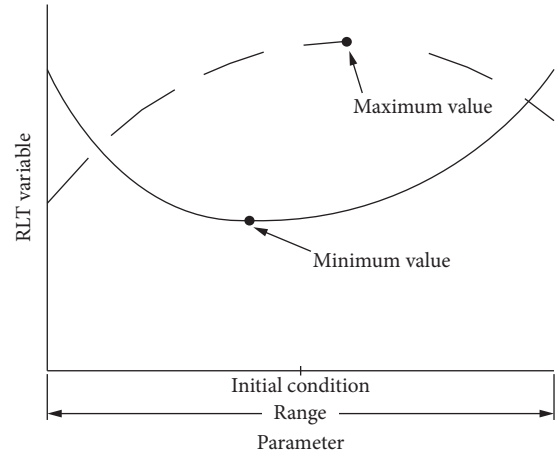

Figure 2: Optimization model.

3. Simulation Model Verification

In the paper, the LJ465Q ethanol-gasoline engine is employed to investigate the optimization research. More specifically, the model is developed by the GT-Power and is used to optimize the manifold length, diameter, and valve timing based on the LJ465Q engine simulation model validated by the experiments, which is beneficial for the improvement of the performance of engine.

3.1. Engine Specifications. The simulation model is shown in Figure 3. Figure 3 shows that the model includes three parts. The left part is the intake system model of LJ465Q engine; the middle part is the intake and exhaust valve, cylinder, and crankcase model. In addition, the right part is the exhaust system model.

3.2. Model Validation. The experiments were carried out on a LJ465Q gasoline engine. The gasoline engine is a four-cylinder, four-stroke, direct injection engine. The main parameters of LJ465Q engine are shown in Table 1. In addition, the inlet valve opening (before top dead center) is 14°CA, the inlet valve closing (after bottom dead center) is 50°CA, the exhaust valve opening (before bottom dead center) is 52°CA, and exhaust valve closing (after top dead center) is 12°CA. The engine test bench is shown in Figure 4. The engine was loaded with a CWF250 electric eddy current dynamometer, and the Kistler pressure sensor was employed to measure the cylinder pressure.

By the field observation, the length, diameter, and bending radius of intake manifold are shown in Figure 5. The section L_1 of intake manifold is an equal diameter, and the diameter is D_1; the section L_2 is the gradient pipeline. The

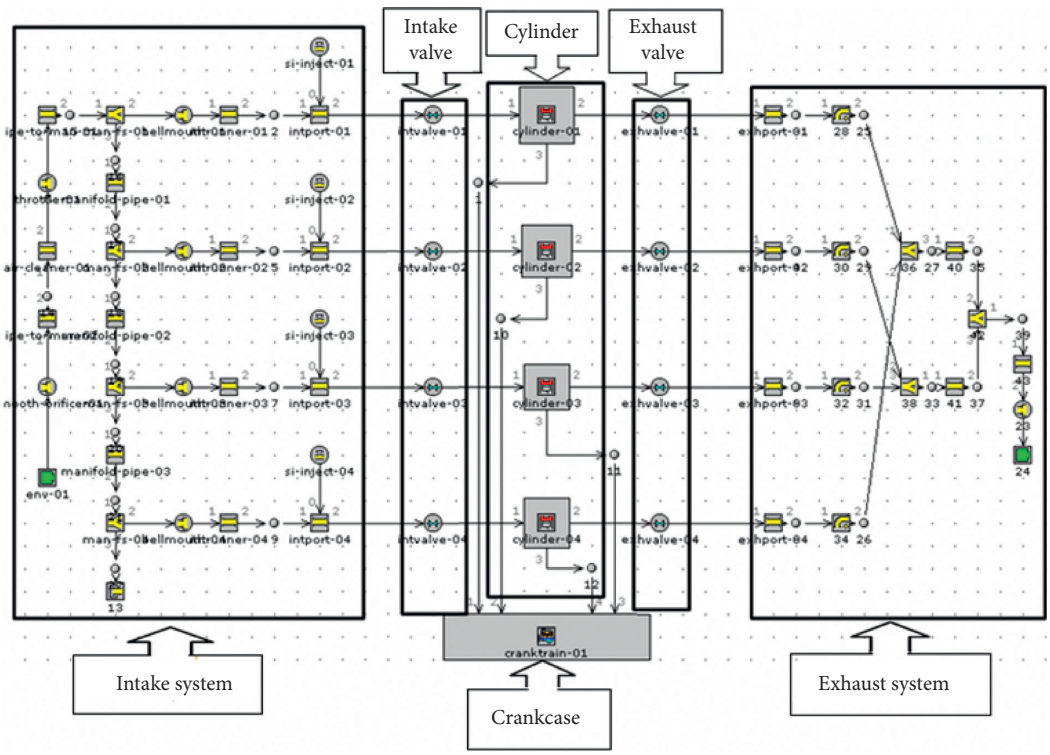

Figure 3: LJ465Q simulation model.

Table 1: Main parameters of LJ465Q engine.

Parameters	Values
Engine type	Four-stroke, in-line, natural inspiration
Displacement (L)	1.051
Bore × stroke (mm)	65.5 × 78
Rate power (kW)	38.5/5200 (r/min)
Compression ratio	9 : 1
Intake manifold total length (mm)	230

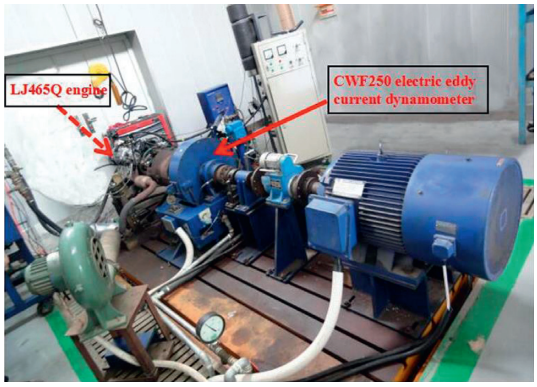

Figure 4: Engine test bench.

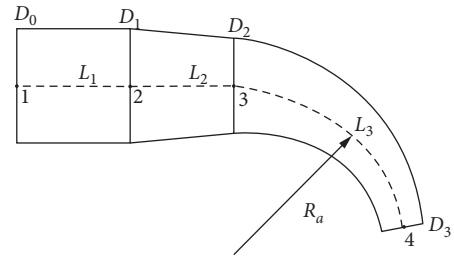

Figure 5: The diagram of intake manifold.

sections of L_2 and L_1 are straight pipes. Thus, the bending radius is infinite, and its value is defined as 10000. The section L_3 is the bend, and the bending angle is $(L_3/R_a) \cdot (180^\circ/\pi)$. In addition, the initial parameters of intake manifold are shown in Table 2. The gas flow in intake manifold is turbulent. According to the directions, the intake manifold is made of cast iron, and the friction coefficient is 0.026.

The power-, torque-, and brake-specific fuel consumption (BSFC) of the engine are shown in Figures 6–8 at full load. It can be found that the predicted results are satisfactory with experimental results at different conditions. More specifically, the max. errors of power, torque, and BSFC predicted by the simulation model are 5.2%, 3.5%, and

Table 2: The initial parameters of intake manifold.

No.	Length (mm)	Diameter (mm)	Bending radius (mm)
1	$L_1 = 55$	$D_1 = 37$	10000
2	$L_2 = 65$	$D_2 = 35$	10000
3	$L_3 = 110$	$D_3 = 30$	Ra

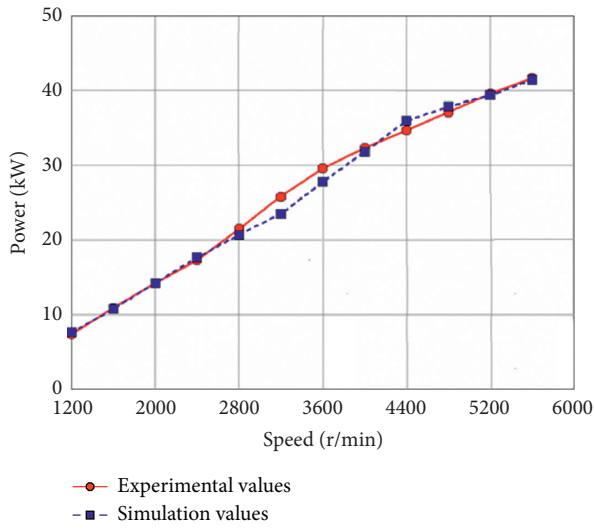

Figure 6: Power comparison.

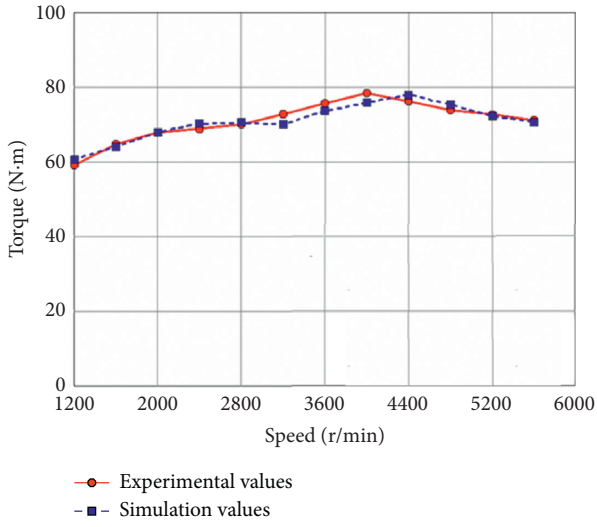

Figure 7: Torque comparison.

7.1%. The engine power increases with the increase in speed. The engine torque firstly increases and then decreases with the increase in speed. In addition, the brake-specific fuel consumption rate of engine is relatively large at low speed. It is due to the simplified simulation of the engine in the simulation process. The lengths of the engine intake and intake pipe are discretized based on the empirical value in the simulation process. As the spraying and burning models

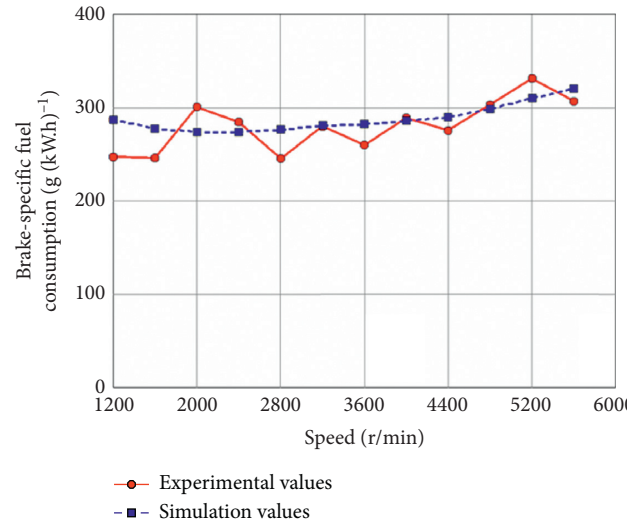

Figure 8: BSFC comparison.

applied in simulation are empirical ones, there are some errors in the actual engine working process. Because of error superposition, the calculated brake-specific fuel consumption rate has some errors, which is less than 7%. The general trend of smaller errors at medium speed is in good agreement with the experimental values. Based on the above analysis, the simulation model has high accuracy and can be applied to simulate and analyze engine performance.

4. Optimization Analysis

In order to achieve the optimization goal of gasoline engine, the engine power and BSFC should be reduced, and the intake efficiency should be improved. Thus, the parameters of the engine performance index (including power-, torque-, and brake-specific fuel consumption and volumetric efficiency) are defined as the result variables of the optimization model, while the parameters of independent variables (including intake and exhaust timing, intake manifold length, and diameter) are taken as the independent variables of the counterpart.

4.1. Effect of Intake Manifold Length on Engine Performance. The air flow and intake port improvement on four valves engine is very important. It directly affects the quality of combustion in cylinder. Thus, the effect of intake manifold length variation in engine performance should be studied. In the paper, it is beneficial to analyzing the influence of intake manifold length change in volumetric efficiency, power, torque, and BSFC when the valve timing and intake manifold diameter keep constant. The original length of intake manifold is 230 mm. The comparisons of volumetric efficiency power, torque, and BSFC with different lengths of intake manifold are shown in Figures 9–12 .

Figure 9 shows that the length of intake manifold also has little influence on the volumetric efficiency of the engine at low speed below 3000 r/min. However, when engine speed

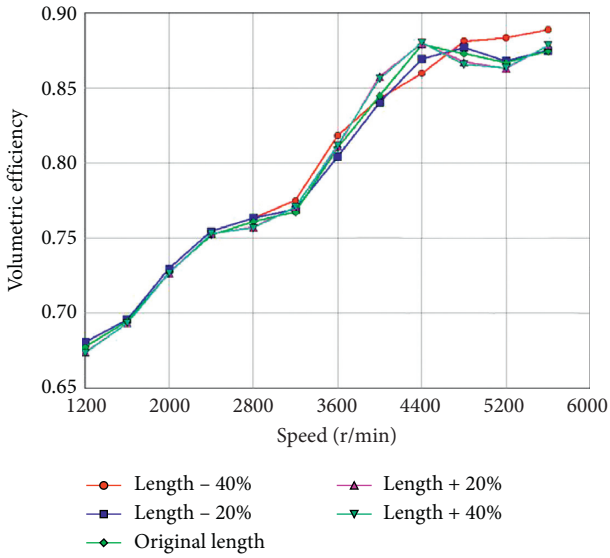

Figure 9: The influence of intake manifold length on volumetric efficiency.

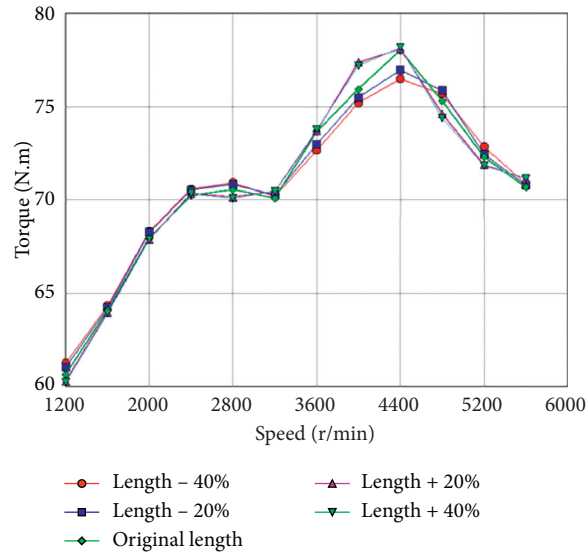

Figure 11: The influence of intake manifold length on torque.

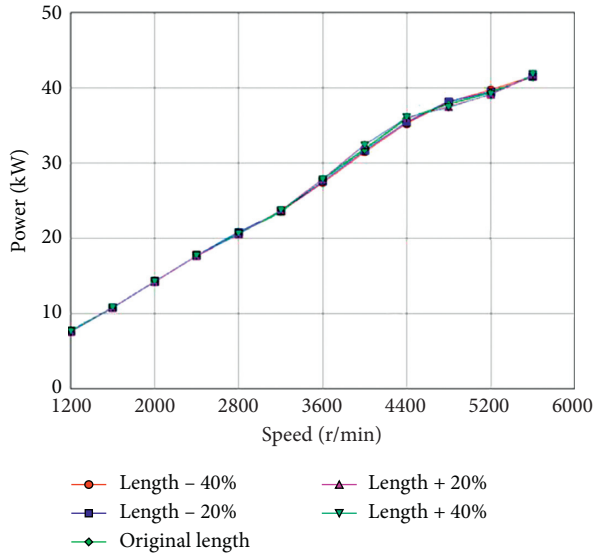

Figure 10: The influence of intake manifold length on power.

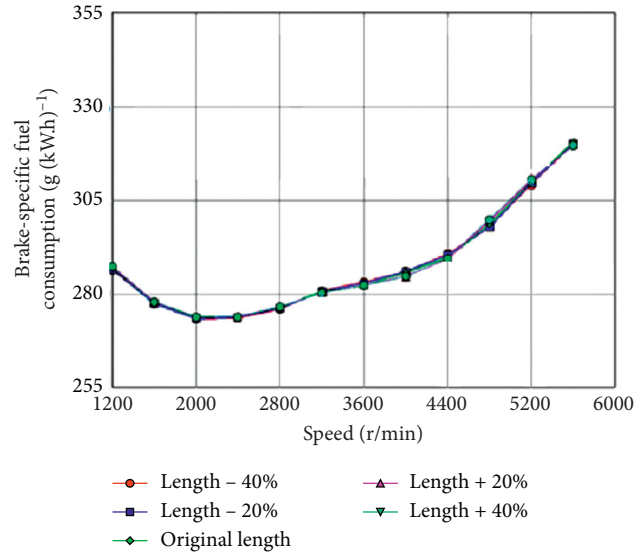

Figure 12: The influence of intake manifold length on BSFC.

is higher than 4000 r/min, the longer the intake manifold is, the faster the volumetric efficiency increases, where the maximum volumetric efficiency of the long scheme appears earlier than that of the short scheme. It is due to the fact that the engine high-speed resonance point corresponds to a higher speed. When intake manifold length increases, high-speed resonance point will move to low speed, which is conducive to the dynamic performance of the engine at medium speed.

Observed from Figures 10 to 12, the simulation results indicate that length of intake manifold has little influence on engine power and BSFC. For instance, the maximum variation in power is 1.6% at the speed of 4400 r/min and the maximum variation in power is 1.4% at the speed of 4800 r/min.

In addition, when the engine speed exceeds 4400 r/min, the volumetric efficiency of the long manifold scheme decreases obviously. It is due to the fact that the volumetric efficiency is affected by the resistance along the pipe. The resistance not only reduces the kinetic energy of fluctuation effect but also attenuates the pressure wave. Similarly, the heat is generated by the friction, resulting in the increase in intake temperature and the reduction in the fresh mixtures into the cylinder.

4.2. Effect of Intake Manifold Diameter on Engine Performance. In the section, six cases are employed to analyzing the influence of intake manifold diameter variation in volumetric efficiency, power, torque, and BSFC when

the valve timing and intake manifold length keep constant. The work cases are shown in Table 3. The original length of intake manifold is 230 mm. The comparisons of volumetric efficiency power, torque, and BSFC with different lengths of intake manifold are shown in Figures 13–16 .

Figures 13–16 show that the length of intake manifold has little influence on engine performance index at low speed, while the performance index changes obviously with the increase in intake manifold diameter at high speed. At high speed, the engine power with the small intake manifold diameter is slightly higher than the engine power with the large intake manifold diameter; for instance, at the speed of 4400 rpm, the engine powers are 38.5 and 36.54 kW when the intake manifold diameters are 24 and 39 mm, respectively. However, the former volumetric efficiency is 4.5% higher than that of the latter. At the same time, the brake-specific fuel consumption rate with the large intake manifold diameter is slightly higher than that with small manifold diameter, and the maximum range is only 1%. It can be found that the performance indexes change obviously when the diameter of intake manifold is less than 30 mm and the performance indexes change little with the increase in the diameter when the diameter of intake manifold is greater than 30 mm.

4.3. Intake System Optimization with Optimization Model. According to the influence trend of structural parameters on volumetric efficiency, based on the GT-Power and optimization model, the length and diameter of intake manifold are taken as independent variables and the volumetric efficiency is defined as the optimization objective value. The proper valve timing of LJ465Q gasoline engine at different speeds is calculated [24]. The improvement of valve timing is very important. It directly affects the quality of combustion in cylinder. Thus, it is very interesting to study the optimal valve timing at different speeds.

4.3.1. Optimization Analysis of Intake Manifold. Figure 17 shows the comparison of volumetric efficiency for different intake manifold lengths and diameters. It can be found that the engine volumetric efficiency is the largest when the diameter D_3 of intake manifold is between 27 mm and 28 mm; the engine volumetric efficiency becomes smaller when the diameter D_3 of intake manifold is larger than 30 mm. From the analysis of flow characteristics of intake manifold, it can be found that the length of intake manifold is also one of the most important factors affecting the volumetric efficiency of the air intake system [25]; for instance, the engine volumetric efficiency is the highest when the length of intake manifold is between 240 mm and 250 mm. In addition, the air intake fluctuation effect is better utilized when the length of intake manifold is 243 mm ($q_1 = 10.5$). In order to meet the requirements of a higher speed on volumetric efficiency, the length and diameter D_3 of intake manifold should be set up to be 243 mm and 28 mm, respectively.

The comparisons of original and optimized dynamic performance are shown in Figure 18 and Table 4.

Table 3: Work cases.

Item	D_3 (mm)	D_2 (mm)	D_1 (mm)
Case 1	24	29	31
Case 2	27	32	34
Case 3	30	35	37
Case 4	33	38	40
Case 5	36	41	43
Case 6	39	44	46

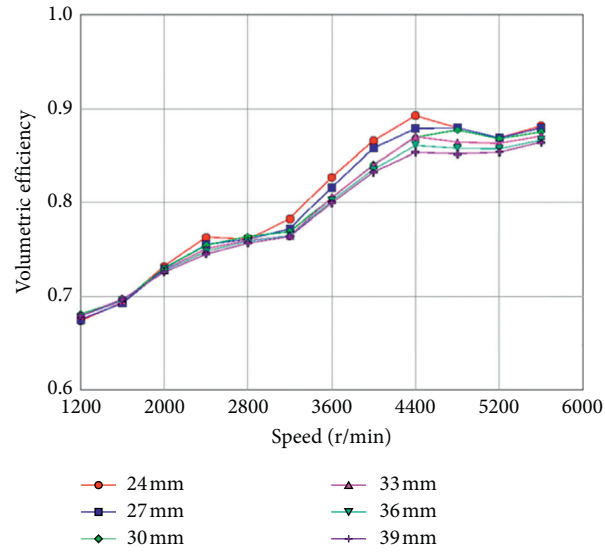

Figure 13: The influence of intake manifold diameter on volumetric efficiency.

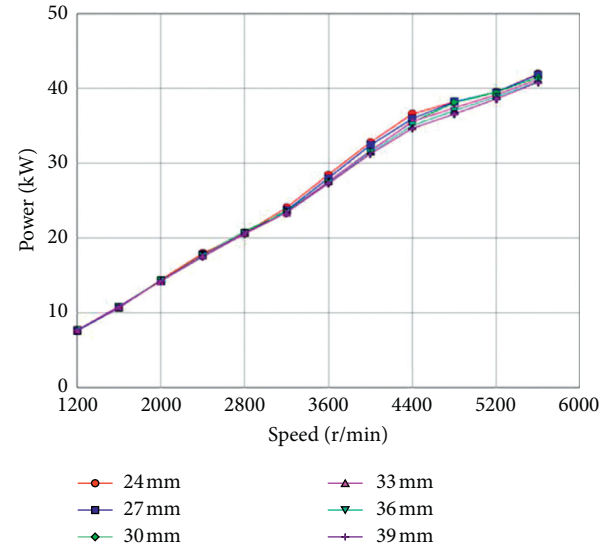

Figure 14: The influence of intake manifold diameter on power.

Figure 18 shows that volumetric efficiency of the engine increases significantly at medium speed. In addition, Table 4 shows that the dynamic performance of the engine is improved, especially at medium speed; for instance, the

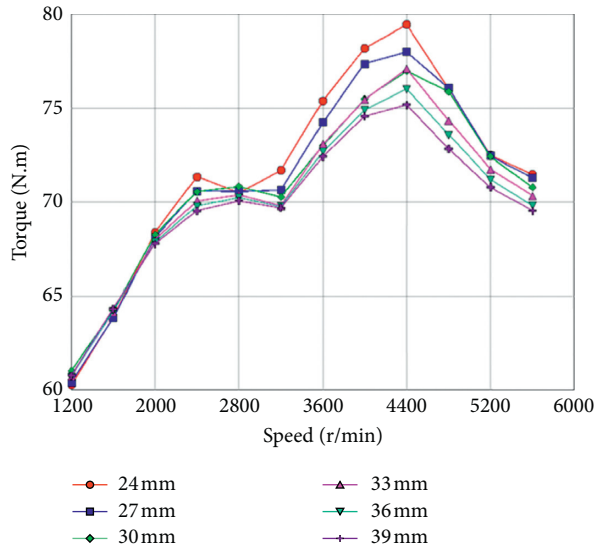

Figure 15: The influence of intake manifold diameter on torque.

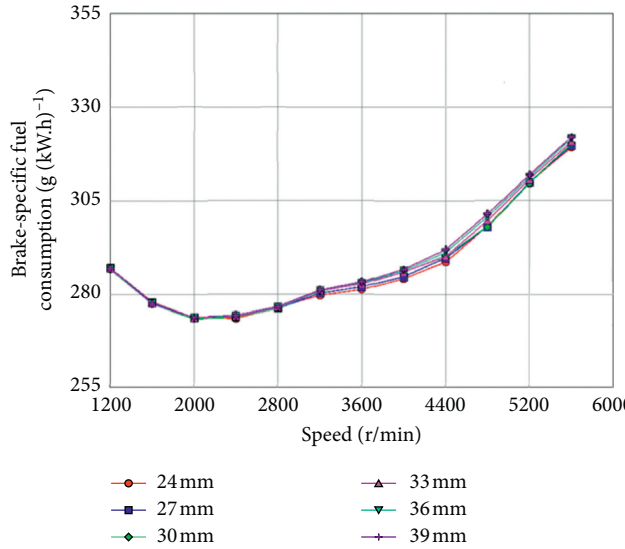

Figure 16: The influence of intake manifold diameter on BSFC.

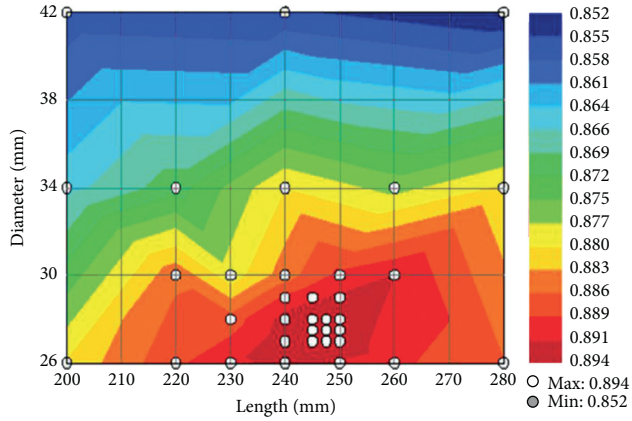

Figure 17: The results of intake manifold structure on the volumetric efficiency.

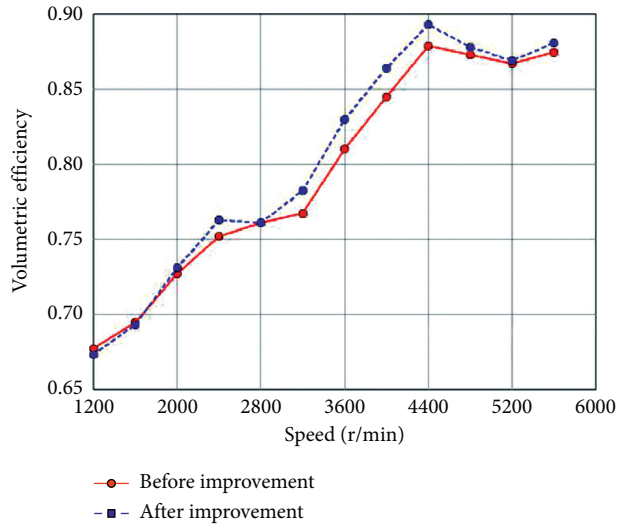

Figure 18: Volumetric efficiency comparison between original and optimized.

Table 4: The comparisons of original and optimized dynamic performance.

Speed (r/min)	Optimized		Original		Increase rate	
	Power (kW)	Torque (N·m)	Power (kW)	Torque (N·m)	Power (%)	Torque (%)
1200	7.57	60.21	7.62	60.62	−0.69	−0.69
1600	10.70	63.88	10.74	64.10	−0.34	−0.34
2000	14.30	68.27	14.23	67.93	0.51	0.51
2400	17.93	71.35	17.65	70.21	1.63	1.63
2800	20.66	70.47	20.68	70.52	−0.07	−0.08
3200	24.03	71.72	23.48	70.08	2.34	2.34
3600	28.54	75.70	27.77	73.65	2.79	2.79
4000	32.66	77.96	31.80	75.92	2.69	2.69
4400	36.63	79.51	35.93	77.99	1.95	1.95
4800	38.11	75.81	37.85	75.30	0.69	0.69
5200	39.48	72.49	39.37	72.29	0.28	0.28
5600	41.85	71.37	41.44	70.67	0.99	0.99

maximum increase in power is 2.79% at the speed of 3600 r/min. At low speed, the dynamic performance is reduced to a certain extent, and the maximum reduction in power reaches 0.69% at the speed of 1200 r/min. It is due to the fact that the valve timing of the engine is fixed. The position of the pressure peak is different at different speeds, and the late angle of intake is perfect at the end of the intake, where the maximum inertia of the intake flow (that is, the pressure wave) arrives at its peak at the through-point of intake valve.

Determining the optimal valve timing of the fixed valve timing mechanism, firstly, the dynamic performance usually should be guaranteed at high speed. The part of the dynamic performance will be inevitably lost at low speed. If the variable valve timing technology is applied, the dynamic performance at low speed can be considered.

4.3.2. Optimization Analysis of Valve Timing. In the low-speed region of engine, the power of valve timing fixed mechanism is insufficient. Thus, the variable valve timing technology can be employed to solve the problem of insufficient power. This method can keep the cam profile unchanged and shift the valve timing to realize the variable valve timing technology. Variable valve timing can be set up by GT-power at its setting module "Cam Timing Angle (°CaA)." The original "Cam Timing Angle" of intake valve is 234.5°CaA and that of exhaust valve is 125°CaA. The "optimizer" module is applied in the simulation of valve timing due to the engine performance affected by the intake and exhaust valves. The variables are the "Cam Timing Angle" at intake and exhaust valves. Thus, the volumetric efficiency is considered as the simulation target. The simulation range is set up to "±20°CaA" with its step size at "2°CaA."

Table 5 shows the simulation results obtained by the improved VVT model at different speeds under external characteristics. Figures 19 and 20 show simulation results of 4400 r/min and 2000 r/min, respectively.

The original and optimized comparisons at full load are shown in Figures 21–24.

Figures 21 to 24 show that the BSFC of the engine improved by variable valve timing is not significant compared with that of the original result, but its volumetric

Table 5: Calculated results of VVT.

Speed (r/min)	Intake timing		Exhaust timing	
	Original	Optimized	Original	Optimized
1200	234.5	225.5	125	120
1600	234.5	227	125	121
2000	234.5	228	125	122
2400	234.5	230	125	122
2800	234.5	230	125	122
3200	234.5	230	125	123
3600	234.5	230	125	123
4000	234.5	227	125	126
4400	234.5	234	125	125
4800	234.5	234.5	125	127
5200	234.5	236	125	126
5600	234.5	237	125	126

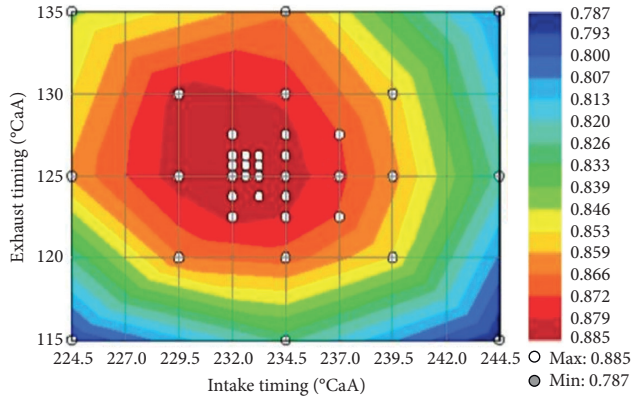

Figure 19: The results of Cam Timing Angle on the volumetric efficiency at 4400 r/min.

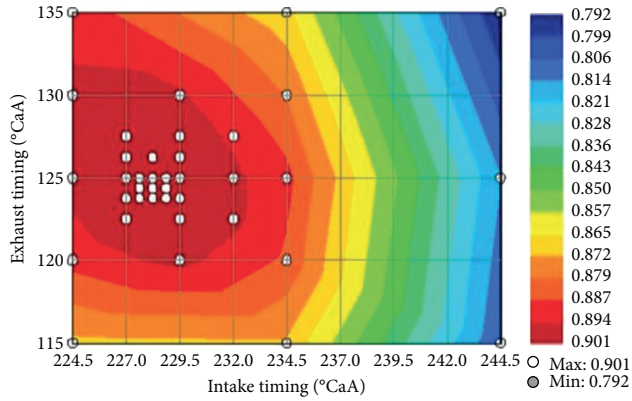

Figure 20: The results of Cam Timing Angle on the volumetric efficiency at 2000 r/min.

efficiency and dynamic performance are significantly improved at low speed; for instance, the maximum increase in power increased by 7.46% at the speed of 1200 r/min. At high speed, the maximum power and torque only slightly increased, not as significant as that at low speed. The optimization of intake manifold structure parameters and the application of variable valve timing technology can improve engine power performance.

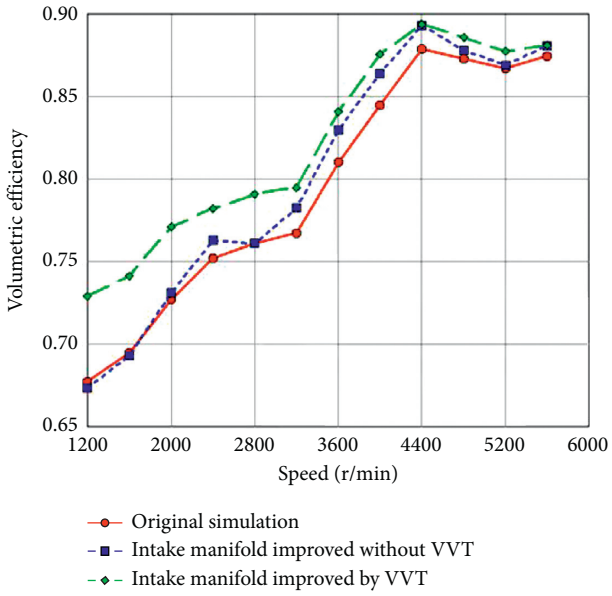

Figure 21: Comparison of original and optimized volumetric efficiency.

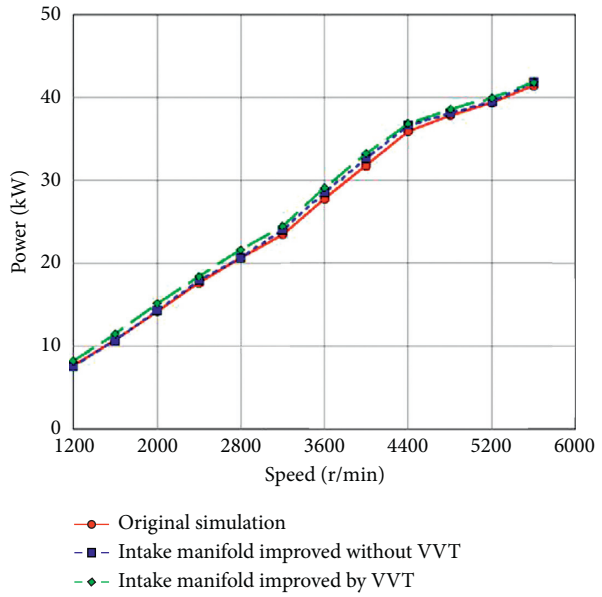

Figure 22: Power comparison between original and optimized.

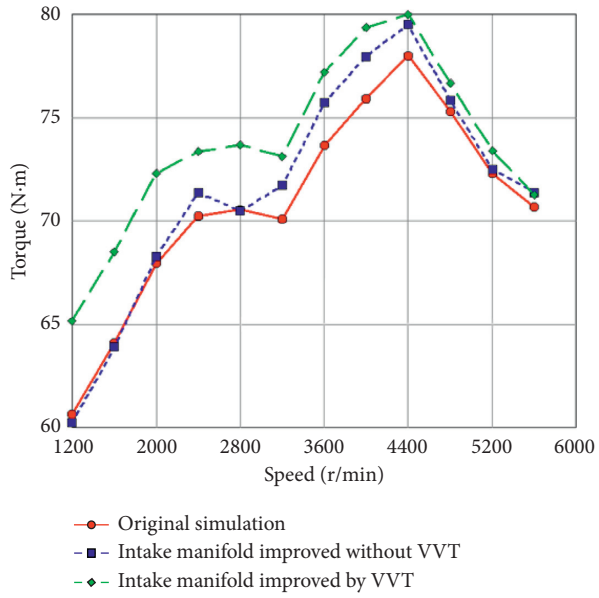

Figure 23: Torque comparison between original and optimized.

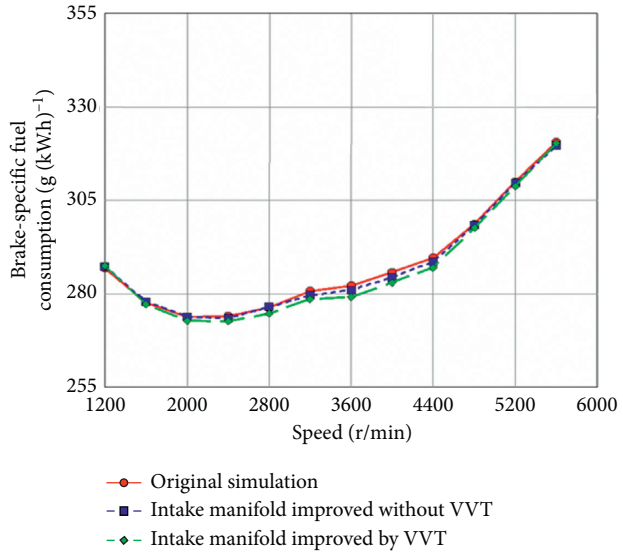

Figure 24: Comparison of the original and optimized BSFC.

5. Conclusion

Today, the environmental pollution [37–41] and energy crisis [7, 13, 42–46] have to learn another new problem. Therefore, an optimization model of four-cylinder gasoline engine was developed by the GT-Power coupled with Matlab-Simulink and was employed to study the optimization of intake system. In order to improve the performance, the engine power-, torque-, and brake-specific fuel consumption are defined as the result variables of the optimization model and the length and diameter of the intake manifold are defined as the independent variables of the model. The reasonable length and diameter of the intake manifold are beneficial to the improvement of engine performance, and the variable intake and exhaust timing method can improve the volumetric efficiency of the engine. The main conclusions are as follows:

(1) The simulation results indicate that the length of intake manifold has little influence on engine power and BSFC. The maximum variation in power is 1.6%, and the maximum variation of power is 1.4%. In addition, when engine speed is higher than 4000 r/min, the longer the intake manifold is, the faster the volumetric efficiency increases.

(2) The length of intake manifold has a great impact on the performance index changes at high speed. At

high speed, the engine power with the small intake manifold diameter is slightly higher than the engine power with the large intake manifold diameter.

(3) The engine volumetric efficiency is the highest when the length of intake manifold is in the range of 240 and 250 mm.

(4) The engine BSFC improved by variable valve timing is not significant compared with that of the original result, but its volumetric efficiency and dynamic performance are significantly improved at low speed. The maximum increase in power increased by 7.46%.

Thus, this research method can be applied to the problems with extreme values [47–48] in the given range of independent variables in the engineering field.

Nomenclature

A: Heat exchange area, m^2
a: Sound velocity of the gas in intake pipe, m/s
C_1: Velocity coefficient
C_2: Combustion chamber status quo coefficient
C_m: Average piston speed, m/s
D: Cylinder diameter, mm
F_3: Cross-sectional area of the intake pipe outlet, m^2
f_1: Natural frequency of pressure wave
f_2: Volumetric frequency
g_f: Circulating fuel injection quantity of the engine, kg/cycle
k: Number of cylinders
L: Intake pipe length, mm
M: Combustion quality index
m: Mass of working fluid in the system, kg
m_{3A}: Mass of the working fluid discharged from the cylinder into the intake pipe, kg
m_B: Instantaneous fuel mass injected into the cylinder, kg
m_e: Mass of exhaust gas flowing out of the cylinder, kg
m_s: Mass of air flowing into the cylinder, kg
n: Engine speed, r/min
P_e: Output power, kW
p: Working fluid pressure, MPa
p_0: Cylinder pressure when the engine is motoring, MPa
p_3: Gas pressure in the intake pipe, MPa
p_a: Working fluid pressure in the cylinder at the starting point of compression, MPa
Q_B: Heat released by the combustion of working fluid in the cylinder, J
Q_W: Heat exchanged through the system boundary, J
R: Gas constant
R_a: Intake pipe radius, mm
T: Working fluid temperature, K
T_a: Temperature in the cylinder at the starting point of compression, K
T_W: Average wall temperature, K
T_{tq}: Torque, N·m
U: Internal energy of the system, J
V: Volume of working fluid in the system, m^3
V_a: Cylinder volume in the cylinder at the starting point of compression, m^3
V_s: Cylinder working volume, m^3
X: Percentage of fuel combustion in the cylinder
W: Mechanical work, J
α_g: Average heat transfer coefficient, $W/(m^2 \cdot K)$
η: Mechanical efficiency
κ_3: Specific heat capacity ratio of the gas in the intake pipe
μ_3: Gas flow coefficient of the intake pipe
ρ_3: Gas density in the intake pipe, kg/m^3
φ: Instantaneous timing angle, °CA
φ_b: Combustion start angle, °
φ_c: Combustion end angle, °
φ_B: Intake valve timing angle, °CA
φ_C: Exhaust valve timing angle, °CA
φ_z: Combustion duration angle, °
ω: Crankshaft speed, r/min.

Data Availability

The data used to support the findings of this study are included within the article and are available from the corresponding author upon request.

Conflicts of Interest

The authors declare that there are no conflicts of interest regarding the publication of this paper.

Acknowledgments

This research was financially supported by the National Natural Science Foundation of China (Grant no. 61963006), Guangxi Natural Science Foundation (Grant nos. 2018GXNSFAA294085 and 2018GXNSFAA050029), and Natural Science Foundation of Guangxi University of Science and Technology (Grant no. 1711309). The authors gratefully acknowledge support from Dr. Juan Wang in the computing.

References

[1] J. E, G. Liu, Z. Zhang et al., "Effect analysis on cold starting performance enhancement of a diesel engine fueled with biodiesel fuel based on an improved thermodynamic model," *Applied Energy*, vol. 243, pp. 321–335, 2019.

[2] J. E, X. Zhao, G. Liu et al., "Effects analysis on optimal microwave energy consumption in the heating process of composite regeneration for the diesel particulate filter," *Applied Energy*, vol. 254, p. 113736, 2019.

[3] Z. Zhang, J. Ye, D. Tan et al., "The effects of Fe2O3 based DOC and SCR catalyst on the combustion and emission characteristics of a diesel engine fueled with biodiesel," *Fuel*, vol. 290, p. 120039, 2021.

[4] G. Wu, Z. Lu, W. Pan, Y. Guan, S. Li, and C. Z. Ji, "Experimental demonstration of mitigating self-excited combustion oscillations using an electrical heater," *Applied Energy*, vol. 239, pp. 331–342, 2019.

[5] H. Zuo, J. Tan, K. Wei, Z. Huang, D. Zhong, and F. Xie, "Effects of different poses and wind speeds on wind-induced vibration characteristics of a dish solar concentrator system," *Renewable Energy*, vol. 168, pp. 1308–1326, 2021.

[6] H. Zuo, G. Liu, J. E et al., "Catastrophic analysis on the stability of a large dish solar thermal power generation system with wind-induced vibration," *Solar Energy*, vol. 183, pp. 40–49, 2019.

[7] F. Zhang, G. Liao, J. E, J. Chen, and E. Leng, "Comparative study on the thermodynamic and economic performance of novel absorption power cycles driven by the waste heat from a supercritical CO2 cycle," *Energy Conversion and Management*, vol. 228, p. 113671, 2021.

[8] Q. Peng, W. Yang, J. E et al., "Investigation on H2/air combustion with C3H8 addition in the combustor with part/full porous medium," *Energy Conversion and Management*, vol. 228, p. 113652, 2020.

[9] Z. Zhang, J. E, J. Chen et al., "Effects of boiling heat transfer on the performance enhancement of a medium speed diesel engine fueled with diesel and rapeseed methyl ester," *Applied Thermal Engineering*, vol. 169, p. 114984, 2020.

[10] G. Wu, D. Wu, Y. Li, and L. Meng, "Effect of acetone-n-butanol-ethanol (ABE) as an oxygenate on combustion, performance, and emission characteristics of a spark ignition engine," *Journal of Chemistry*, vol. 2020, Article ID 7468651, 11 pages, 2020.

[11] Z. Zhang, J. E, Y. Deng et al., "Effects of fatty acid methyl esters proportion on combustion and emission characteristics of a biodiesel fueled marine diesel engine," *Energy Conversion and Management*, vol. 159, pp. 244–253, 2018.

[12] T. Liu, J. E, W. M. Yang et al., "Investigation on the applicability for reaction rates adjustment of the optimized biodiesel skeletal mechanism," *Energy*, vol. 150, pp. 1031–1038, 2018.

[13] K. Wei, Y. Yang, H. Zuo, and D. Zhong, "A review on ice detection technology and ice elimination technology for wind turbine," *Wind Energy*, vol. 23, no. 3, pp. 433–457, 2019.

[14] J. Fan, Y. Wu, A. Ohata, and T. Shen, "Conservation law-based air mass flow calculation in engine intake systems," *Science China Information Sciences*, vol. 59, no. 11, p. 112210, 2016.

[15] L. V. Plotnikov, B. P. Zhilkin, and Y. M. Brodov, "The influence of piston internal combustion engines intake and exhaust systems configuration on local heat transfer," *Procedia Engineering*, vol. 206, pp. 80–85, 2017.

[16] E. Yilmaz, M. Ichiyanagi, and T. Suzuki, "Development of heat transfer model at intake system of IC engine with consideration of backflow gas effect," *International Journal of Automotive Technology*, vol. 20, no. 5, pp. 1065–1071, 2019.

[17] D. Di Battista, M. Di Bartolomeo, and R. Cipollone, "Flow and thermal management of engine intake air for fuel and emissions saving," *Energy Conversion and Management*, vol. 173, pp. 46–55, 2018.

[18] J. E, M. Pham, D. Zhao et al., "Effect of different technologies on combustion and emissions of the diesel engine fueled with biodiesel: a review," *Renewable and Sustainable Energy Reviews*, vol. 80, pp. 620–647, 2017.

[19] B. Zhang, J. E, J. Gong, W. Yuan, X. Zhao, and W. Hu, "Influence of structural and operating factors on performance degradation of the diesel particulate filter based on composite regeneration," *Applied Thermal Engineering*, vol. 121, pp. 838–852, 2017.

[20] D. Han, J. E, Y. Deng et al., "A review of studies using hydrocarbon adsorption material for reducing hydrocarbon emissions from cold start of gasoline engine," *Renewable and Sustainable Energy Reviews*, vol. 135, p. 110079, 2021.

[21] X. Chen, Z. Wang, S. Pan, and H. Pan, "Improvement of engine performance and emissions by biomass oil filter in diesel engine," *Fuel*, vol. 235, pp. 603–609, 2019.

[22] B. Zhang, Y. Tang, and Z. Shen, "Investigations on the soot combustion performance enhancement of an improved catalytic gasoline particulate filter regeneration system under different electric heating powers," *Fuel*, vol. 283, p. 119301, 2021.

[23] R. C. Costa, S. D. M. Hanriot, and J. R. Sodré, "Influence of intake pipe length and diameter on the performance of a spark ignition engine," *Journal of the Brazilian Society of Mechanical Sciences and Engineering*, vol. 36, no. 1, pp. 29–35, 2014.

[24] B. Zhang, H. Zuo, Z. Huang, J. Tan, and Q. Zuo, "Endpoint forecast of different diesel-biodiesel soot filtration process in diesel particulate filters considering ash deposition," *Fuel*, vol. 272, p. 117678, 2020.

[25] M. Mourad and K. Mahmoud, "Investigation into SI engine performance characteristics and emissions fuelled with ethanol/butanol-gasoline blends," *Renewable Energy*, vol. 143, pp. 762–771, 2019.

[26] X. Yang, C. Liao, and J. Liu, "Harmonic analysis and optimization of the intake system of a gasoline engine using GT-power," *Energy Procedia*, vol. 14, pp. 756–762, 2012.

[27] Y. L. Qi, L. C. Dong, H. Liu, P. V. Puzinauskas, and K. C. Midkiff, "Optimization of intake port design for SI engine," *International Journal of Automotive Technology*, vol. 13, no. 6, pp. 861–872, 2012.

[28] D. B. Pai, H. S. Singh, and P. V. F. Muhammed, "Simulation based approach for optimization of intake manifold," SAE, Warrendale, PA, USA, Technical Papers 2011-26-0074, 2011.

[29] E. A. A. Silva, A. A. V. Ochoa, and J. R. Henríquez, "Analysis and runners length optimization of the intake manifold of a 4-cylinder spark ignition engine," *Energy Conversion and Management*, vol. 188, pp. 310–320, 2019.

[30] S. Guo, S. Huang, and M. Chi, "Optimized design of engine intake manifold based on 3D scanner of reverse Engineering," *EURASIP Journal on Image and Video Processing*, vol. 70, 2018.

[31] P. Carvalho, A. Piccini, A. Goulart, F. Balbom, and A. Müller, "Design and optimization of the intake system of a formula sae race engine," SAE, Warrendale, PA, USA, Technical Papers 2019-36-0253, 2020.

[32] Y. Sun, T. Wang, Z. Lu, L. Cui, and M. Jia, "The optimization of intake port using genetic algorithm and artificial neural network for gasoline engines," SAE, Warrendale, PA, USA, Technical Papers 2015-01-1353, 2015.

[33] T. J. Wang, "Optimum design for intake and exhaust system of a heavy-duty diesel engine by using DFSS methodology," *Journal of Mechanical Science and Technology*, vol. 32, no. 7, pp. 3465–3472, 2018.

[34] G. Wu, X. Wang, S. Abubakar, Y. Li, and Z. Liu, "A realistic skeletal mechanism for the oxidation of biodiesel surrogate composed of long carbon chain and polyunsaturated compounds," *Fuel*, vol. 289, p. 119934, 2021.

[35] Z. Zhang, J. E, J. Chen et al., "Effects of low-level water addition on spray, combustion and emission characteristics of a medium speed diesel engine fueled with biodiesel fuel," *Fuel*, vol. 239, pp. 245–262, 2019.

[36] F. Zhou, J. Fu, W. Ke, J. Liu, Z. Yuan, and B. Luo, "Effects of lean combustion coupling with intake tumble on economy and emission performance of gasoline engine," *Energy*, vol. 133, pp. 366–379, 2017.

[37] Y. Xie, Q. Zuo, M. Wang et al., "Effects analysis on soot combustion performance enhancement of an improved

catalytic gasoline particulate filter regeneration system with electric heating," *Fuel*, vol. 290, p. 119975, 2021.

[38] E. Jiaqiang, P. Zheng, D. Han, X. Zhao, and Y. Deng, "Effects analysis on soot combustion performance enhancement in a rotary diesel particulate filter unit during continuous microwave heating," *Fuel*, vol. 276, p. 118043, 2020.

[39] B. Zhang, J. E, J. Gong et al., "Multidisciplinary design optimization of the diesel particulate filter in the composite regeneration process," *Applied Energy*, vol. 181, pp. 14–28, 2016.

[40] E. Jiaqiang, M. Zhao, Q. Zuo et al., "Effects analysis on diesel soot continuous regeneration performance of a rotary microwave-assisted regeneration diesel particulate filter," *Fuel*, vol. 260, p. 116353, 2020.

[41] E. Jiaqiang, X. Zhao, L. Xie et al., "Performance enhancement of microwave assisted regeneration in a wall-flow diesel particulate filter based on field synergy theory," *Energy*, vol. 169, pp. 719–729, 2019.

[42] W. Zuo, E. Jiaqiang, and R. Lin, "Numerical investigations on an improved counterflow double-channel micro combustor fueled with hydrogen for enhancing thermal performance," *Energy Conversion and Management*, vol. 159, pp. 163–174, 2018.

[43] Q. Peng, W. Yang, J. E et al., "Investigation on H2/air combustion with C3H8 addition in the combustor with part/full porous medium," *Energy Conversion and Management*, vol. 228, p. 113652, 2021.

[44] Q. Peng, W. Yang, J. E et al., "Effects of propane addition and burner scale on the combustion characteristics and working performance," *Applied Energy*, vol. 285, p. 116484, 2021.

[45] Y. DengW. Zheng et al., "Influence of geometric characteristics of a diesel particulate filter on its behavior in equilibrium state," *Applied Thermal Engineering*, vol. 123, pp. 61–73, 2017.

[46] Y. DengJ. Cui et al., "Investigations on the temperature distribution of the diesel particulate filter in the thermal regeneration process and its field synergy analysis," *Applied Thermal Engineering*, vol. 123, pp. 92–102, 2017.

[47] D. Tan, Z. Chen, J. Li et al., "Effects of swirl and boiling heat transfer on the performance enhancement and emission reduction for a medium diesel engine fueled with biodiesel," *Processes*, vol. 9, no. 3, p. 568, 2021.

[48] X. Zhao, E. Jiaqiang, G. Liao, F. Zhang, J. Chen, Y. Deng et al., "Numerical simulation study on soot continuous regeneration combustion model of diesel particulate filter under exhaust gas heavy load," *Fuel*, vol. 290, p. 119795, 2021.